Computerized Medical Imaging and Graphics 35 (2011) 315–323

Contents lists available at ScienceDirect

Computerized Medical Imaging and Graphics

journal homepage: www.elsevier.com/locate/compmedimag

Neural network based focal liver lesion diagnosis using ultrasound images

Deepti Mittal[a,*], Vinod Kumar[a], Suresh Chandra Saxena[a], Niranjan Khandelwal[b], Naveen Kalra[b]

[a] Department of Electrical Engineering, Indian Institute of Technology Roorkee, Roorkee 247667, Uttarakhand, India
[b] Department of Radiodiagnosis, Postgraduate Institute of Medical Education and Research, Chandigarh 160012, India

ARTICLE INFO

Article history:
Received 4 August 2010
Received in revised form
21 December 2010
Accepted 24 January 2011

Keywords:
Ultrasound
Focal liver lesions
Feature extraction
Classification
Neural network classifier

ABSTRACT

Present study proposes a computer-aided diagnostic system to assist radiologists in identifying focal liver lesions in B-mode ultrasound images. The proposed system can be used to discriminate focal liver diseases such as Cyst, Hemangioma, Hepatocellular carcinoma and Metastases, along with Normal liver. The study is performed with 111 real ultrasound images comprising of 65 typical and 46 atypical images, which were taken from 88 subjects. These images are first enhanced and then regions of interest are segmented into 800 non-overlapping segmented regions-of-interest. Subsequently 208-texture based features are extracted from each segmented region-of-interest. A two step neural network classifier is designed for classification of five liver image categories. In the first step, a neural network classifier gives classification among five liver image categories. If neural network decision is for more than one class as obtained from the first step, binary neural network classifiers are used in the second step for crisp classification between two classes. Test results of two-step neural network classifier showed correct decisions of 432 out of 500 segmented regions-of-interest in test set with classification accuracy of 86.4%. The classifier has given correct diagnosis of 90.3% (308/340) in the tested segmented regions-of-interest from typical cases and 77.5% (124/160) in tested segmented regions-of-interest from atypical cases.

1. Introduction

Focal liver lesions pose a diagnostic challenge to radiologist and clinician alike. Ultrasound (US) is the most widespread non-invasive imaging modality for screening focal liver lesions because of its low cost and real-time imaging capabilities. Noninvasive diagnosis (detection and characterization) of focal liver lesions is also carried out by computerized tomography and magnetic resonance, but these imaging modalities are of higher cost, having a lack of real-time imaging and greater operational inconvenience in comparison to US images. The B-mode US that is generally the first-choice imaging technique for the liver has serious limitations in detection and characterization of focal lesions [1]. These limitations are (i) the poor sensitivity in detection of solid lesions with a false-negative rate of more than 50%, (ii) low or absent contrast between the lesion and the surrounding liver (so-called iso-echoic lesions) and (iii) overlapping of sonographic visual information resulting in overlapping among ranges of focal lesions in features extracted from the gray scale image. Therefore, it is desirable to reduce these limitations in order to improve the diagnostic accuracy of focal liver lesions based on conventional B-mode US images.

Experienced radiologists visualize the various sonographic features in liver US images to characterize the focal lesions and Normal (NOR) liver tissues. In liver US images, typical appearance of Cyst is anechoic with distal acoustic enhancement and thin imperceptible walls, as shown in Fig. 1(a). Hemangioma (HEM) is the most common benign tumor of the liver. It affects the liver's blood vessels. HEM can have a wide range of sonographic appearance. Typical HEMs are hyperechoic to normal liver and their texture patterns are homogeneous as shown in Fig. 1(b). The large sized HEMs show varied imaging features due to internal hemorrhage and fibrosis. The most common primary malignant liver tumor is Hepatocellular carcinoma (HCC). Typically, these lesions appear hypoechoic with heterogeneous texture on US as shown in Fig. 1(c). A small HCC can be hypoechoic and homogeneous. Metastases (MET) are the most common malignant liver neoplasms and can originate from many different types of cancer. Typically, MET may undergo liquefactive necrosis, producing a fluid centre with an internal texture pattern often inhomogeneous as shown in Fig. 1(d). In US images, it may appear cystic, hypo-, iso- or hyperechoic. NOR liver tissues have isoechoic appearance and homogeneous texture and it is shown in Fig. 1(e). These visually extractable features are based on echogenicity and echo texture pattern. In most cases, the sonographic appearance of HEM, HCC and MET overlaps sufficiently to make a distinction difficult or impossible.

US sensitivity for the depiction of MET is low (50–77%) due to inability of US to detect small or iso-echoic lesions [2]. HEM having

* Corresponding author. Tel.: +91 9412363054.
E-mail address: deeptimit@gmail.com (D. Mittal).

0895-6111/$ – see front matter © 2011 Elsevier Ltd. All rights reserved.
doi:10.1016/j.compmedimag.2011.01.007

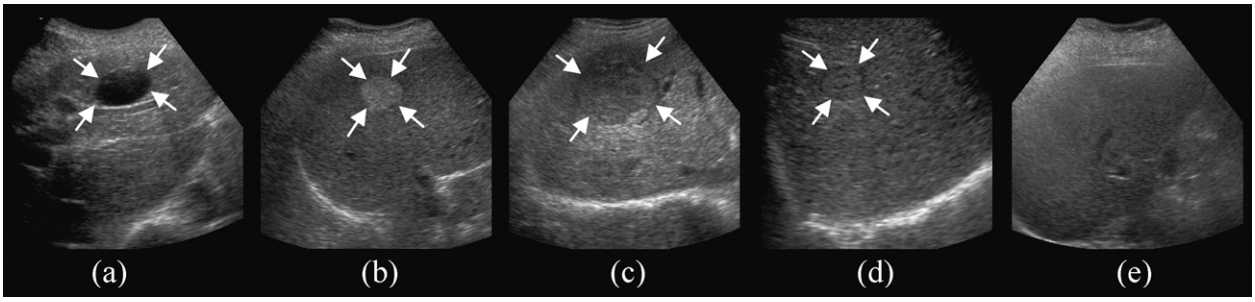

Fig. 1. Ultrasound liver images with typical appearance of (a) Cyst, (b) Hemangioma, (c) Hepatocellular carcinoma, (d) Metastases, and (e) Normal liver.

size less than 1 cm^2, are usually indistinguishable from small MET on unenhanced US. In the clinical context, the relatively low contrast between MET and adjacent liver tissue reduces the effective resolution of US imaging methods by a factor of 10 or more [3]. Developments in US that may improve the differentiation between liver lesions along with NOR liver tissues include the application of power Doppler, ultrasonic contrast agents and harmonic imaging. Alternatively, a texture enhancement strategy of the B-mode US images can improve the diagnosis.

The studies on characterization and classification of US focal liver lesions are few and they are given in Table 1 for a comparative study. Sujana et al. [4] have classified benign and malignant focal diseases with NOR liver by neural network (NN) classifier using 11 texture features on a limited image set. Yoshida et al. [5] have applied multiscale texture analysis for distinguishing benign from malignant focal liver lesions with a database of 44 patients. Poonguzhali and Ravindran [6] have classified NOR, Cyst, benign and malignant masses with a small image set using various statistical and spectral features. Kim et al. [7] employed computerized schemes and radiologists' grading to test different types of image features of focal liver lesions. Finally, they concluded high correlation between the characteristics of clinical diagnosis and computerized analysis. It supports that echogenicity and texture characteristics provide the best suitable mathematical feature descriptors for characterization of focal liver lesions.

The studies reported so far reveals that there has been no attempt to classify HCC (primary cancer) and MET (secondary cancer). Therefore, the present classification study is concentrated on classification among five liver image classes including four common focal liver lesions along with NOR liver tissues with a set of 111 images of 88 patients. These focal lesions are (i) Cyst (liquid nodule), (ii) HEM (non-cancerous solid nodule), (iii) HCC (primary cancerous solid nodule) and (iv) MET (secondary cancerous solid nodule). A focal liver lesion with its typical appearances can be identified easily by the radiologists. However, the presence of atypical appearances/features in a focal liver lesion may lead to misdiagnosis and confusion with other lesions even for the expert radiologists. Thus, the study includes both typical and atypical cases of focal lesions. Further, to extract the subtle sonographic information, the contrast of the US image is enhanced by using a new methodology as proposed by authors of present work [8].

In the present work, large numbers of features are extracted by using statistical, spectral and TEM methods to maximally discriminate the focal lesions by developing a NN classification system. A NN classification system mimics the human reasoning and in some cases, it gives the decision for more than one class to show the possibilities of other diseases. Thus to help radiologists to decide for

Table 1
Brief detail of the studies on classification of focal liver lesions.

Author (year)	Liver image classes	Image database		No. of SROIs		SROIs distribution for NN classifier		
		Patients	Images per class			Train set	Test set	
Sujana (1996)	1- Hemangioma	-		113	Hemangioma	(15)	(5)	
	2- Malignant				Malignant	(30)	(10)	
	3- Normal				Normal	(40)	(13)	
Author (year)	Liver image classes	Image database		No. of SROIs		SROIs distribution for NN classifier		
		Patients	Images per class			Cross Validation procedure		
Yoshida (2003)	1- Benign (Hemangioma)	44	Hemangioma (17)	193	Hemangioma	(50)		
	2- Malignant		HCC (11)		HCC	(87)		
	(HCC+ Metastases)		Metastases (16)		Metastases	(56)		
Poonguzhalli (2008)	1- Cyst	-		160	Cyst	(40)		
	2- Benign				Benign	(40)		
	3- Malignant				Metastases	(40)		
	4- Normal				Normal	(40)		
Author (year)	Liver image classes	Image database		No. of SROIs		SROIs distribution for NN classifier		
		Patients	Images per class			Train set	Validation set	Test set
Present study (2010)	1- Cyst	88	Cyst (17)	800	Cyst	(50)	(10)	(6)
	2- HCC		HCC(15)		HCC	(50)	(10)	(167)
	3- Hemangioma		Hemangioma (18)		Hemangioma	(50)	(10)	(30)
	4- Metastases		Metastases (45)		Metastases	(50)	(10)	(125)
	5- Normal		Normal (16)		Normal	(50)	(10)	(172)

the one most probable class in these cases, a new approach of two step NN classifier is developed to classify the focal liver disease with high performance.

2. Materials and methods

2.1. Materials

In this research, 111 B-mode US images comprising 16 normal liver images, 17 Cyst, 15 HCC, 18 HEM and 45 MET were collected from the Department of Radiodiagnosis, Postgraduate Institute of Medical Education & Research (PGIMER), Chandigarh, India. These US images were acquired from 88 different patients: 52 men (mean age: 52 years), 35 women (mean age: 44 years) and 1 child (age: 8 years) with an age range from 8 to 85 years over the time period March 2008 to May 2009. The consents of patients for using these images for research were taken prior to image recording. The study was approved by the medical ethics committee of the PGIMER, Chandigarh. All images were obtained using the same US equipment (Philips ATL HDI 5000 ultrasound scanner) with multi-frequency transducer of 2–5 MHz range. All images had their own clinical setting.

Histological characteristics of US images in present study were confirmed by the expert radiologists. Radiologists' liver image assessment criteria include (i) their knowledge and experienced based visual image interpretation of focal liver diseases, (ii) clinical history of a patient, and (iii) disease confirmation by the biopsy/dynamic helical CT/MRI/pathological examinations.

US liver image set have 95 liver images of focal lesions. These images are marked by an expert radiologist for both typical and atypical cases of focal liver lesions. Out of 111 US image, 24 images (2 Cyst, 3 HCC, 8 HEM, 11 MET) are of atypical cases and rest 87 images (15 Cyst, 12 HCC, 10 HEM, 34 MET) are from typical cases.

2.2. Methods

The proposed system as shown in Fig. 2 first enhances the clinically acquired US images, then marked regions of interest (ROIs) by the radiologist in these images are segmented into segmented regions-of-interest (SROIs). The system further consists of two modules: (i) the feature extraction module and (ii) the classification module. SROIs are fed to the feature extraction module and passed to the classification module. Classification module has two step of NN implementation and they are shown in Fig. 3. MATLAB 7.5 is used to implement the NN classifier. All datasets are stored in a PC (Pentium Dual-Core 2.67 GHz with 1.97 GB RAM).

2.2.1. Image enhancement

In order to improve the efficiency and veracity of diagnosis, it is very essential to have good quality of images. Clinically acquired US images have limited soft tissue contrast and inherent speckle formation that impose limitations on the diagnostic performance of B-scan US images. Experienced radiologists visualize the texture of the US images in order to discriminate among focal liver lesions. Speckle is integral part of texture in US images. Therefore, to improve the visualization of US images, speckle reduction process is applied in such a way that the visual details of the texture should remain preserved. This is done by using diamond shape template, having forty neighborhood pixels, to calculate diffusion term in speckle reduction anisotropic diffusion scheme and the contrast of US images is enhanced by incorporating nonquadratic regularization in diffusion term [8]. This methodology simultaneously operates both an enhancement and speckle-reduction process, and it can optimally enhance an US image. The enhancement of images was approved and confirmed by visual interpretations of two expert radiologists. Fig. 4 shows images of all five liver image classes and their enhanced counterparts. Fig. 4A1, B1, C1, D1, and E1 are original images of Cyst, HCC, HEM, MET, and NOR liver tissues, respectively, and Fig. 4A2, B2, C2, D2, and E2 are corresponding enhanced images in terms of contrast. Circled regions in Fig. 4 show the lesions. Texture contrast of the lesion is better visualized in enhanced images in comparison to corresponding original images of HCC, HEM and MET. Cyst is clearly distinct with its surroundings in enhanced image in comparison to the original image. A better NOR image contrast is also observed in comparison to the corresponding original image (Fig. 4E1) as shown in Fig. 4E2.

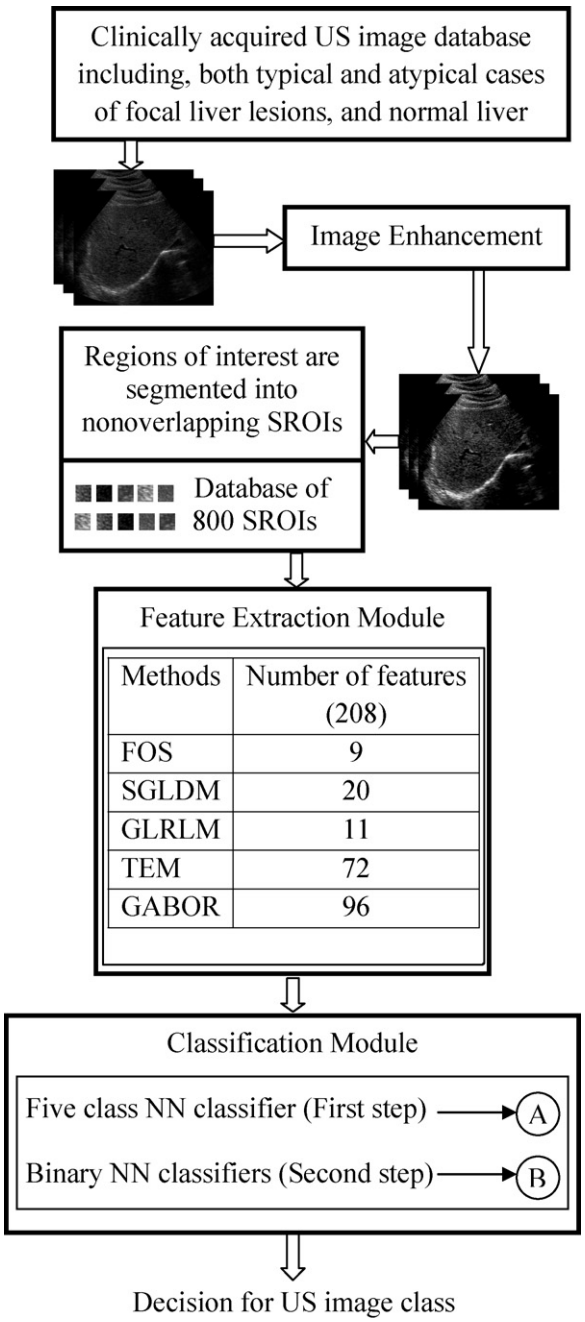

Fig. 2. The computer-aided diagnostic system for ultrasound focal liver diseases.

2.2.2. Segmentation of region-of-interest

ROIs of liver lesion area are marked by an expert radiologist. These marked ROIs are segmented into maximum possible number of non-overlapping 25×25 sized small ROIs termed as segmented regions-of-interest (SROIs). A SROI is inside the lesion and it should avoid the margins of the lesion. SROI does not include major vas-

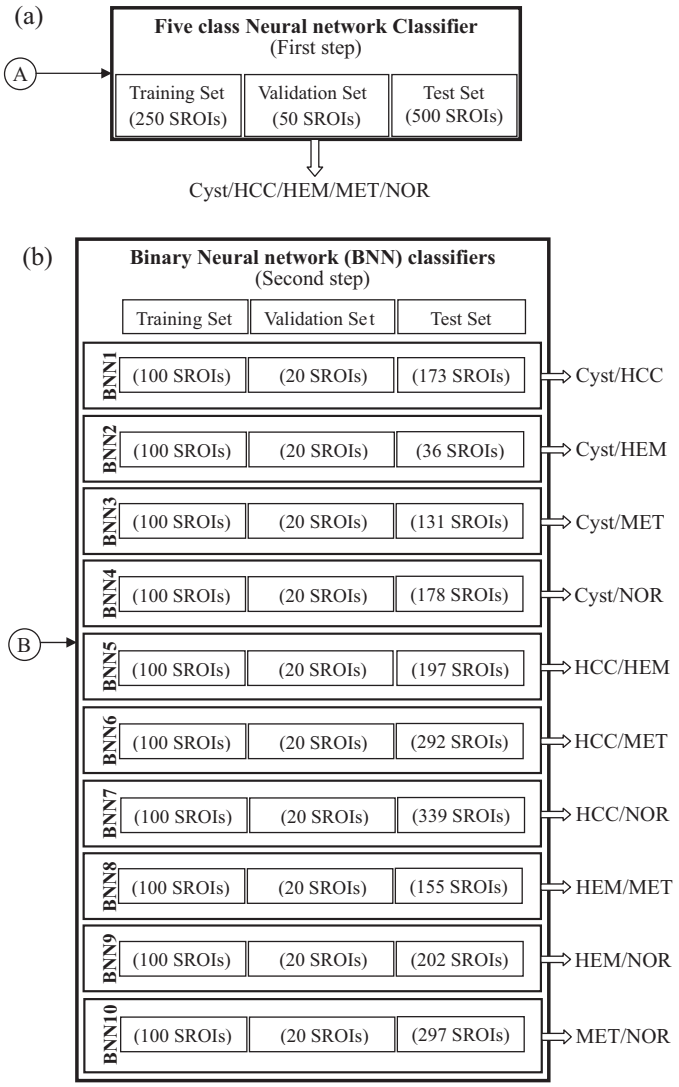

Fig. 3. Two steps of classification module: (a) five class neural network classifier; (b) binary neural network classifiers.

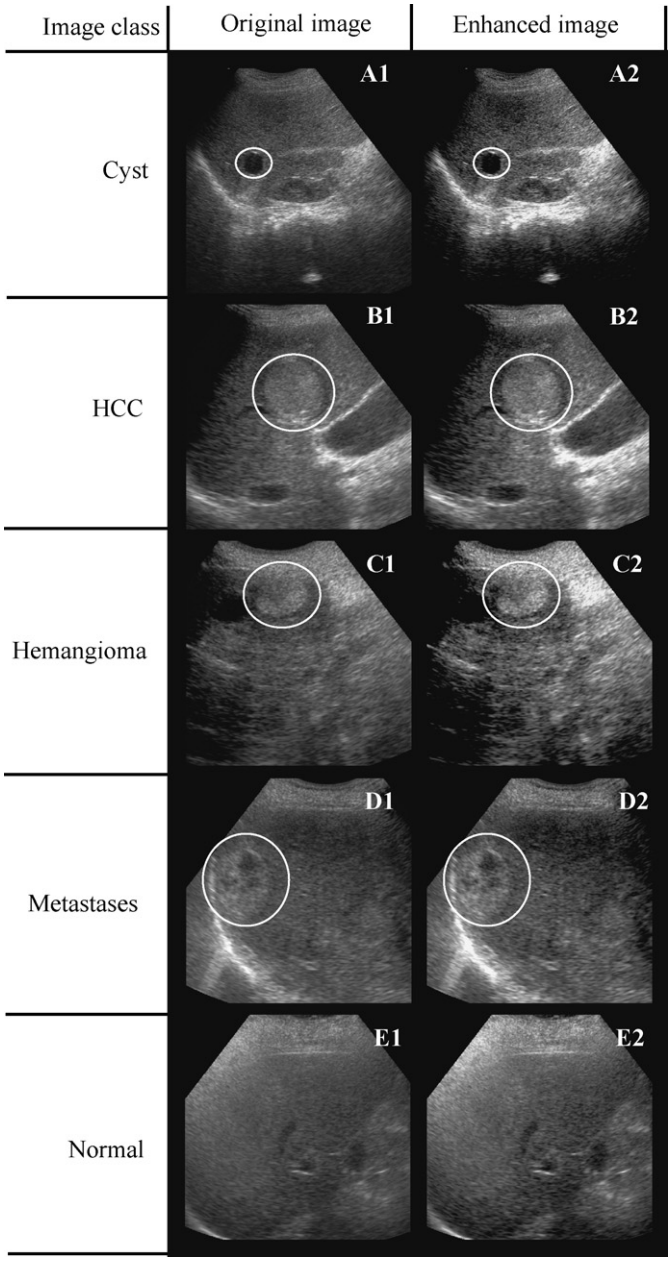

Fig. 4. Original and enhanced ultrasound images of five liver image categories.

cular structures in the ROIs. Sujana et al. [4] and Poonguzhali and Ravindran [6] have used SROI of the size of 10×10 pixels for the study of focal liver lesions, whereas Yoshida et al. [5] have used SROI of the size of 60×60 pixels. Texture parameters are considered sensitive to the size of SROI. Therefore, SROI should have enough number of pixels to provide a good statistical population. Also, the size of SROI should be small enough to be able to segment even the minimum sized lesion ROI. Different SROI sizes are tested to optimize the performance with the available image set. The size of 10×10 pixels is small enough to provide a good statistical population and size of 60×60 pixels is bigger to segment most of the liver lesions that are smaller than this size. After trail and interaction with two radiologists, ROIs of 25×25 pixels were selected for the present study.

2.2.3. Feature extraction module

Radiologists according to their clinical experience assess focal soft tissue masses in liver US images using echogenicity and visual echotexture criteria. Feature of echogenicity is strengthened after contrast enhancement in the discrimination task between five liver image classes. Echotexture is frequently used analysis to extract various distinguishing features to discriminate between liver image classes. A good number of visual and non-visual echotexture features are explored and then applied in the present classification study with the tedious task of assembling the effective features.

Statistical analysis of texture, computes features at each point in an image, and derives a set of statistics from the variety of features. A feature is combination of intensities at specific positions relative to each point in the image. According to the number of points which define a feature, statistics are classified into first-order, second-order and higher-order statistics. These statistics provide various measures of textural properties. The spectral methods provide frequency content based descriptions. Out of the wide categories of spectral methods multi-resolution analysis approach by Gabor wavelet, and spatial filtering based descriptors e.g. Laws' texture energy mask are frequently used methodologies in the literatures [6,9–13]. In present study, initially texture features from five widely used methods of first, second and higher order statistics, spatial filtering and multiresolutional approaches are selected. These methods are named as (i) first order statistics (FOS), (ii) spatial gray level dependence matrix (SGLDM), (iii) gray level run length matrix

Table 2
Tabulation of one-dimensional filters of lengths 5, 7, and 9 used in driving the texture energy features and the number of corresponding rotation invariant features.

Filter resolution type by filter length	1-D convolution filters	Number of 2-D filter mask generated from 1-D filters (N)	Number of filter pairs having one filter in the pair identical to other if one of them is rotated by 90° (M)	Number of rotational invariant images ($N-M$)
Length 5	L5 = [1, 4, 6, 4, 1] E5 = [−1, −2, 0, 2, 1] S5 = [−1, 0, 2, 0, −1] W5 = [−1, 2, 0, −2, 1] R5 = [1, −4, 6, −4, 1]	25	10	15
Length 7	L7 = [1, 6, 15, 20, 15, 6, 1] E7 = [−1, −4, −5, 0, 5, 4, 1] S7 = [−1, −2, 1, 4, 1, −2, −1]	9	3	6
Length 9	L9 = [1, 8, 28, 56, 70, 56, 28, 8, 1] E9 = [1, 4, 4, −4, −10, −4, 4, 4, 1] S9 = [1, 0, −4, 0, 6, 0, −4, 0, 1] W9 = [1, −4, 4, 4, −10, 4, 4, −4, 1] R9 = [1, −8, 28, −56, 70, −56, 28, −8, 1]	25	10	15
	Total	59	23	36

(GLRLM), (iv) texture energy measures (TEM) and (v) Gabor wavelet (GWT). The selection of these methods is based on literature studies specifically with US images [6,9–11] and focal liver lesions with US images [4–6]. These studies have used the combinations of various feature extraction methods. Poonguzhali and Ravindran [6] have used SGLDM, GLRLM, TEM and GWT methods with limited feature studies for focal liver diseases classification. In the proposed work, classification study is extended to classify cancer diseases, HCC and MET, along with Cyst, HEM, and NOR liver tissues. Additional textural features are also taken to improve the classification accuracy as compared to Poonguzhali and Ravindran [6]. Therefore with the aim to extract a relevant set of diagnostically important features of proposed disease classification tasks, 208 features are extracted using the five methods, viz., FOS, SGLDM, GLRLM, TEM and GWT methods. These five sets of texture features were calculated from each SROI and combined into one set of features for image characterization. The five sets of texture features are listed as follows.

2.2.3.1. First order statistics (FOS). The nine measures of first-order statistics are selected in the present study [14,15]. These are mean_{FOS}, median_{FOS}, variance_{FOS}, skewness_{FOS}, kurtosis_{FOS}, entropy_{FOS}, mode_{FOS}, $\text{standard\_deviation}_{FOS}$, and range_{FOS}.

2.2.3.2. Spatial gray level dependency matrix (SGLDM). Twenty features are selected using SGLDM for the present study [16–18]. These are autocorrelation, contrast, correlation, cluster prominence, cluster shade, dissimilarity, energy_{SGLDM}, entropy_{SGLDM}, homogeneity, maximum probability, variance_{SGLDM}, sum average, sum variance, sum entropy, difference variance, difference entropy, information measure of correlation 1, information measure of correlation 2, inverse difference normalized, and inverse difference moment normalized.

2.2.3.3. Gray level run-length matrix (GLRLM). The texture features based on GLRLM are short run emphasis, long run emphasis, high gray-level run emphasis, low gray-level run emphasis, short run low gray-level emphasis, short run high gray-level emphasis, long run low gray-level emphasis, long run high gray-level emphasis, gray-level non-uniformity, run length non-uniformity and run percentage [19,20].

2.2.3.4. Texture energy measures (TEM). Law's texture energy measures [21] are derived from one-dimensional filters of length 5, length 7 and length 9 in this work and these filters are shown in Table 2. The different filter lengths are used for different resolutions to extract various image features from SROI images. A total of 59 two-dimensional filters are generated by combining these one-dimensional filters. These two-dimensional filters are used to convolve the SROI images. A 15×15 square window is applied to these convolved images to compute texture energy images. Out of the 59 two-dimensional filters, 23 filters are identical to other 23 filters if they are rotated by 90°. Texture energy images which are computed from such pair of identical filters can be combined as rotation invariant image. For example, image obtained by filter E5L5 can be added with the image obtained by filter L5E5 to obtain rotation invariant image. Thus a total of 36 rotational invariant texture energy images are obtained. Mean and variance are calculated from each rotational invariant texture energy images resulting in overall 72(=36×2) features.

2.2.3.5. Gabor wavelet (GWT). The frequency and orientation selective properties of a Gabor filter are very useful in providing a multiscale texture description [22,23]. Image expansions with the set of Gabor wavelets provide localized frequency descriptions (local features/energies) of image. Four quantitative values such as mean, variance, skewness and entropy are extracted from this group of energy distributions for four scales and six orientations and a set of total ($4 \times 4 \times 6$=) 96 texture features is obtained.

2.2.4. Classification module

Firstly, full feature set was used as an input to a NN based classifier in order to classify SROIs into one of the five classes. The NN consists of an input layer with a number of input neurons equal to the number of the features i.e. 208, one hidden layer and one output layer with five neurons for five classes. In order to find the appropriate number of hidden neurons, a trial-and-error process was applied. Various numbers of hidden neurons were tried, and it was found that twenty neurons in hidden layer were reasonable for classification and fast convergence. The desired output was set to 1 for the output neuron corresponding to the labeled class and 0 for the other output neurons. The learning of the NN was supervised and the weights were adjusted by backpropagation (BP) procedure with adaptive learning rate and momentum in order to obtain a desired input–output relationship.

A three-stage (training–validation–test) methodology is used for the development of classification system with neural network. SROIs are distributed randomly into three disjoint sets: training

Table 3
Confusion matrix on the test results after first step of neural network classifier module.

Class code	Test results after first step of neural network classifier module				
	CYST	HCC	HEM	MET	NOR
CYST	5	5	0	3	0
HCC	1	148	4	7	3
HEM	0	7	18	29	3
MET	0	3	8	81	17
NOR	0	4	0	5	149
Individual class classification accuracy (%)	83.3(5/6)	88.6(148/167)	60.0(18/30)	64.8(81/125)	86.6(149/172)
Overall classification accuracy (%)	80.2(401/500)				

Shaded values show the number of SROIs that are diagnosed correctly.

set, validation set and testing set. The training set, consisting of 250 SROIs having 50 SROIs of each five classes, is used to select the sets of parameters for NN architecture and NN weights. A set of 50 SROIs having 10 SROIs from each liver image class was used for the validation of the trained NN and to identify the NN architecture with the best performance. Once the architecture is selected using the validation set, the parameters of the detection program are fixed. The performance of the program is then evaluated with an independent test set. The testing set consists of rest 500 SROIs (6 corresponding to Cyst, 167 to HCC, 30 to HEM, 125 to MET and 172 to NOR) having uneven distribution of SROIs with liver tissue categories because of the restriction with dataset acquired in the duration of one year.

The NN gives a value (in the range of 0–1) at each output node as a response to the input. This value is a probability (or weightage) for the image class representing that output node. It was observed that out of 500 SROIs of test set, 401 SROIs were correctly classified with highest probability and 99 SROIs were incorrectly classified. Out of these 99 SROIs of misclassification, it was observed that in case of 50 SROIs, correct classification was having probability (output of NN) as next highest probability. Therefore for further improvement of classification accuracy of the NN classifier, the extracted feature set of SROIs that have got highest and next highest probability in the first step of NN classifier were passed through the binary classifier in the second step. For the second step of NN classifier, all possible ten binary classifiers are developed with optimized performance in distinguishing between two classes. The designed classifier performances are tested with the available SROIs in the test set between these two classes. Designing of binary classification module is shown in Fig. 3. Optimized binary neural networks (BNNs) have input layer with 208 units, one hidden layer with 20 units (BNN for Cyst vs. HEM have hidden layer with 15 units), and one output layer with 1 unit.

3. Results and discussion

The proposed NN classifier in the first step was trained for 100% accuracies in classifying SROIs among five liver image classes for both the training and validation set. These accuracy results demonstrate the optimal efficiency of the NN in differentiation among texture data of training and validation set in five liver image classes. Generalized performance of this system is evaluated by the confusion matrices for the test set to indicate that the classification tendency is reasonable.

The results after first step of NN classifier as shown in Table 3, show that out of 500 SROIs, 401 SROIs were classified correctly with an accuracy of 80.2% (401/500). The details of classification results for each class after first step are given in Table 3. The test datasets of Cyst, HCC, HEM, and MET contain 50% (3/6), 34% (52/167), 90% (27/30) and 59% (74/125) atypical SROIs respectively. Both HEM and MET liver tissue classes have more than 50% of atypical SROIs. Therefore, the results of classification with HEM and MET having

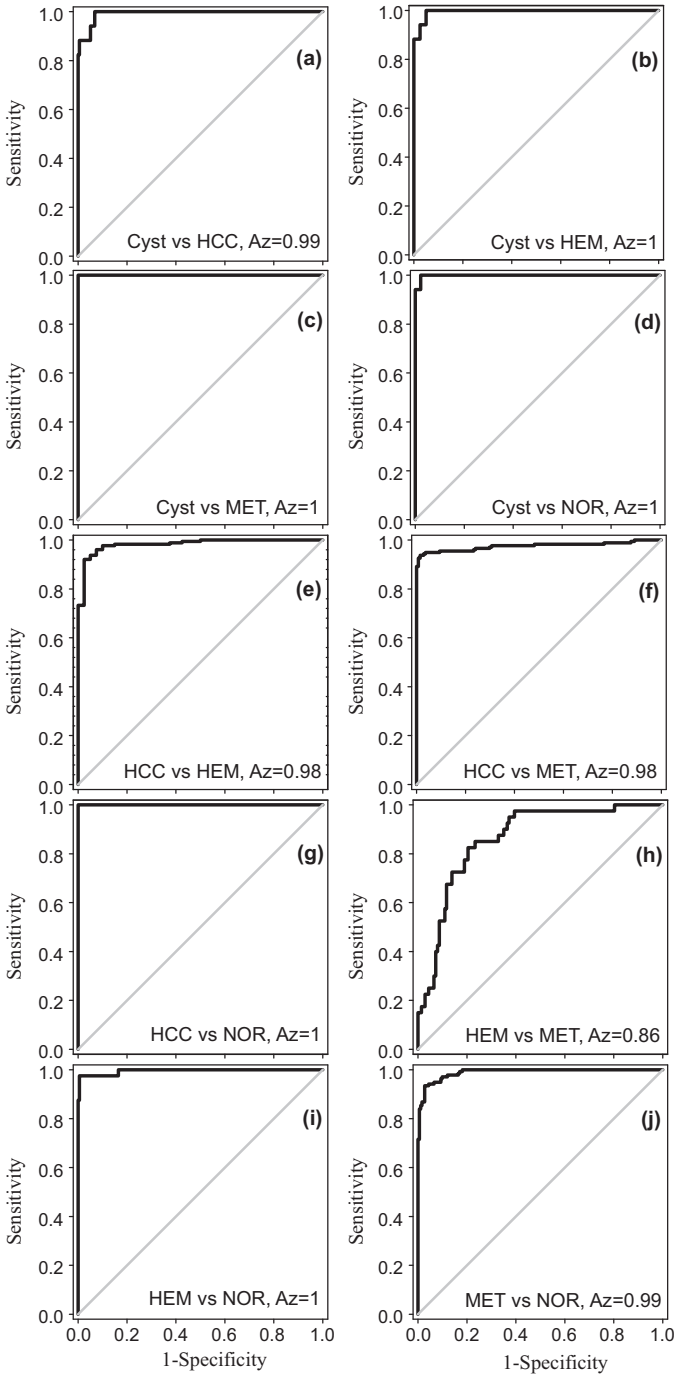

Fig. 5. Receiver operating characteristics curve for binary neural network classifiers.

Table 4
Confusion matrix on the test results after second step of neural network classifier module.

Class code	Test results after second step of neural network classifier				
	CYST	HCC	HEM	MET	NOR
CYST	5	2	0	2	0
HCC	1	155	2	4	0
HEM	0	6	23	25	5
MET	0	3	5	90	8
NOR	0	1	0	4	159
Individual class classification accuracy (%)	83.3(5/6)	92.8(155/167)	76.7(23/30)	72.0(90/125)	92.4(159/172)
Overall classification accuracy (%)	86.4(432/500)				

Table 5
Confusion matrix on the test results after second step of NN classifier module for typical cases.

Class code	SROI samples of testing set (typical cases)				
	CYST	HCC	HEM	MET	NOR
CYST	3	1	0	0	0
HCC	0	103	0	0	0
HEM	0	4	3	10	5
MET	0	2	0	40	8
NOR	0	1	0	1	159
Individual class classification accuracy (%)	100(3/3)	92.8(103/111)	100(3/3)	78.4(40/51)	92.4(159/172)
Overall classification accuracy (%)	90.3(308/340)				

a good percentage of atypical cases in their datasets are poor with accuracy of 60.0% and 64.8% respectively. In addition, HEM dataset has 90% of atypical cases, whereas MET dataset has only 59% of atypical cases. This is the reason that the classification accuracy of HEM (i.e. 60.0%) is even less than that of MET (i.e. 64.0%).

In the second step of NN classifier, ten binary classifiers as shown in Fig. 3 are used. The ability of a classifier to correctly identify positives and negatives is assessed by sensitivity and specificity. A receiver operating characteristics (ROC) curve plots sensitivity vs. specificity across a range of values and its area represents the predictability of a classifier. The performances of the designed binary classifiers are demonstrated with the help of ROC curves and the area under the ROC (A_Z) curves as shown in Fig. 5. A_Z values are 1 for binary classification tasks of Cyst vs. HEM, Cyst vs. MET, Cyst vs. NOR, HCC vs. NOR, and HEM vs. NOR respectively. A_Z values are quite high i.e. 0.99, 0.98, 0.98, 0.86 and 0.99 for rest binary classification tasks of Cyst vs. HCC, HCC vs. HEM, HCC vs. MET, HEM vs. MET and MET vs. NOR respectively.

The generalized performance of the two-step NN classifier is finally evaluated by the confusion matrices for the test set. Table 4 shows the confusion matrix of test results after two step NN classifier for all the five classes. The classification performance for Cyst, HCC, and NOR liver tissues are good with classification accuracy of 83.3%, 92.8%, and 92.4% respectively. Out of 6 SROIs of Cyst 5 are detected correctly and 1 is misclassified as HCC. The failure case of Cyst is an atypical case which has visual characteristic showing good resemblance with HCC, such as variable echogenicity with hypoechoic appearance like HCC lesion. Out of 167 SROIs of HCC, 155 are detected correctly and 12 are misclassified. Similarly for 172 SROIs of NOR liver tissues, 159 are classified correctly. The NN classifier system shows reasonable accuracy of 76.7% and 72.0% for HEM and MET respectively. Thus the overall accuracy of the proposed two-step NN classifier is found to be 86.4%. When this accuracy is compared with the corresponding accuracy after first step of NN classifier, an increment of 6.2% is observed with the detection of 31 more SROIs correctly with the inclusion of binary classification module after first step. It is also observed that NOR cases that are misclassified as HEM are 3 after first step and this misclassification is increased to 5 after second step. The reason is that two normal SROI images that are misclassified as MET in the first step, has its second highest weightage to the HEM class. Therefore, in these two cases a binary classifier in between MET and HEM is selected inside the binary classification module. This gives a wrong selection of binary classifier and leads a wrong final decision for HEM.

The performance of the proposed two-step NN classifier is also evaluated by analyzing the classification accuracies of typical and atypical cases separately for all the classes and these results are

Table 6
Confusion matrix on the test results after second step of NN classifier module for atypical cases.

Class code	SROI samples of testing set (atypical cases)				
	CYST	HCC	HEM	MET	NOR
CYST	2	1	0	2	0
HCC	1	52	2	4	0
HEM	0	2	20	15	0
MET	0	1	5	50	0
NOR	0	0	0	3	0
Individual class classification accuracy (%)	66.7(2/3)	92.7(52/56)	74.1(20/27)	67.6(50/74)	0
Overall classification accuracy (%)	77.5(124/160)				

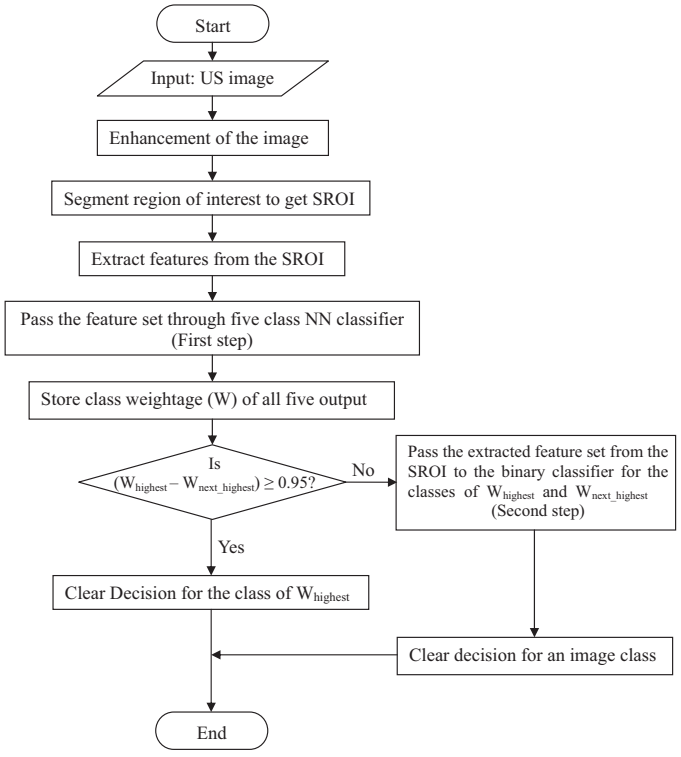

Fig. 6. Flowchart showing the working of proposed CAD system.

given in Tables 5 and 6 respectively. It can be observed from these tables that the proposed classifier gives 90.3% classification accuracy for typical cases and 77.5% for atypical cases.

Finally Fig. 6 shows the working steps of the proposed CAD system. Fig. 6 shows that, if the difference in probability of classification between two classes as output of NN classifier is 0.95 or higher than 0.95, the second step is not required. The output of NN with highest probability can be taken as final classification and it can also save computational time.

4. Conclusion

In this study, a CAD system has been proposed for diagnosis of US focal liver images with attributes like enhancement of US images, 208 texture based features and two-step NN classifier. The performance of the CAD has shown overall accuracy of 86.4% in detection of both typical and atypical test SROIs from focal liver lesions and NOR liver tissues. The proposed NN model is in two stages, accuracy of classification with one stage is 80.2%, by adding a second stage of NN, the classification accuracy has improved to 86.4%. Under the situation where diagnosis of radiologists (atypical cases) is not clear, this two-step NN classifier shows a good performance. The overall classification accuracy with this system has been achieved as 90.3% for typical cases and 77.5% for atypical cases.

References

[1] Cosgrove D. Contrast-enhanced ultrasound in focal liver lesions guidelines for clinicians. Eur Gastroenterol Rev 2008:34–6.
[2] Mathieu D, Luciani A. Imaging update in metastatic liver disease. Controversies Consensus Imaging Interv 2003:21–6.
[3] Robinson PJA. Imaging liver metastases: current limitations and future prospects. Br J Radiol 2000;73:234–41.
[4] Sujana H, Swarnamani S, Suresh S. Application of artificial neural networks for the classification of liver lesions by image texture parameters. Ultrasound Med Biol 1996;22:1177–81.
[5] Yoshida H, Casalino DD, Keserci B, Coskun A, Ozturk O, Savranlar A. Wavelet-packet-based texture analysis for differentiation between benign and malignant liver tumors in ultrasound images. Phys Med Biol 2003;48: 3735–53.
[6] Poonguzhali S, Ravindran G. Automatic classification of focal lesions in ultrasound liver images using combined texture features. Inform Tech J 2008;7:205–9.
[7] Kim SH, Lee JM, Kim KG, Kim JH, Lee JY, Han JK, et al. Computer-aided image analysis of focal hepatic lesions in ultrasonography: preliminary results. Abdom Imaging 2009;34:183–91.
[8] Mittal D, Kumar V, Saxena SC, Khandelwal N, Kalra N. Enhancement of the ultrasound images by modified anisotropic diffusion method. Med Biol Eng Comput 2010;48(12):1281–91.
[9] Christodoulou CI, Pattichis CS, Pantziaris M, Nicolaides A. Texture-based classification of atherosclerotic carotid plaques. IEEE Trans Med Imaging 2003;22(7):902–12.
[10] Stoitsis J, Valavanis I, Mougiakakou SG, Golemati S, Nikita A, Nikita KS. Computer-aided diagnosis based on medical image processing and artificial intelligence methods. Nuclear Inst Meth Phys Res 2006;569:591–5.
[11] Raja KB, Madheswaran M, Thyagarajah K. A hybrid fuzzy-neural system for computer-aided diagnosis of ultrasound kidney images using prominent features. J Med Syst 2008;32:65–83.
[12] Sriraam N, Roopa J, Saranya M, Dhanalakshmi M. Performance evaluation of computer aided diagnostic tool (CAD) for detection of ultrasonic based liver disease. J Med Syst 2009;33:267–74.
[13] Mougiakakou SG, Valavanis IK, Nikita A, Nikita KS. Differential diagnosis of CT focal liver lesions using texture features, feature selection and ensemble driven classifiers. Artif Intell Med 2007;41:25–37.
[14] Golemati S, Tegos TJ, Sassano A, Nikita KS, Nicolaides AN. Echogenicity of B-mode sonographic images of the carotid artery. J Ultrasound Med 2004;23:659–69.
[15] Sonnad SS. Describing data: statistical and graphical methods. Radiology 2002;225:622–8.
[16] Haralick RM, Shanmugam K, Dinstein I. Texture features for image classification. IEEE Trans Syst Man Cybern 1973;SMC-3:610–21.
[17] Soh L, Tsatsoulis C. Texture analysis of SAR sea ice imagery using gray level co-occurrence matrices. IEEE Trans Geosci Remote Sens 1999;37: 780–95.
[18] Clausi DA. An analysis of co-occurrence texture statistics as a function of grey level quantization. Can J Remote Sens 2002;28:45–62.
[19] Galloway MM, Texture analysis using gray level run lengths. Comp Graph Image Process 1975;4:172–9.
[20] Tang X. Texture information in run-length matrices. IEEE Trans Image Process 1998;7(11):1602–9.
[21] Laws KI. Rapid texture identification. SPIE 1980;238:376–80.
[22] Manjunath BS, Ma WY. Texture features for browsing and retrieval of image data. IEEE Trans Pattern Anal Mach Intell 1996;18:837–42.
[23] Arivazhagan S, Ganesan L, Priyal SP. Texture classification using Gabor wavelets based rotation invariant features. Pattern Recog Lett 2006;27:1976–82.

Deepti Mittal was born in Moradabad, on March 8, 1976. She received the B.Tech. degree in Electronics Engg from Harcourt Butler Technological Institute, Kanpur, and M.Tech. (Hons.) degree in Electronics & Communication Engg. from Govind Ballabh Pant University of Agriculture & Technology, Pantnagar in 1999, and 2004 respectively. She worked as a Lecturer/Lecturer (Senior Scale) in Department of Electronics Engineering, Moradabad Institute of Technology, Moradabad from September 1999 to February 2007. At present she is pursuing her Ph.D. degree in Electrical Engineering Department, Indian Institute of Technology Roorkee. She taught UG/PG courses related to electronics and communication engineering. She is a life member of Indian Society for Technical Education and The Institution of Electronics and Telecommunication Engineers. Her professional research interests are in Image Processing, in particular applied to biomedical applications.

Vinod Kumar obtained his B.Sc. (Electrical Engineering) Hons degree from Punjab University in 1973, ME (Measurement & Instrumentation) Hons and Ph.D. degree from University of Roorkee in 1975 and 1984 respectively. He joined the Electrical Engineering Department of University of Rookee (presently, IIT Roorkee) in 1975 and is presently Professor & Head in Electrical Engineering Department of Indian Institute of Technology Roorkee. He has guided 15 doctoral and more than 80 Master's theses and has more than 150 research publications in internationally reputed Journals and Conference proceedings. He has undertaken large number of consultancy and sponsored projects from industries and government departments. He holds membership of many professional bodies. He is a fellow of the Institute of Engineers (I), Institution of Electronics and Telecommunication Engineers and member of Biomedical Engineering Society of India. He is a Senior Member of IEEE, USA. He has many honors and awards to his credit, namely IETE – K S Krishna Memorial Award, The Railway Board's Prize: by Institution of Engineers (I), The Brijmohan Memorial Prize by Institution of Engineers (I), Outstanding Teacher's Award during by IIT Roorkee, Khosla Cash Award & Prize, Khosla Cash Prize, Khosla Annual Research Prize, Certificate of Merit for research papers by Institution of Engineers (I), IETE – R S Khandpur Gold Medal for life-time achievements and outstanding contribution at national/international level in the field of 'Medical Instrumentation'. He has also conducted several courses, workshops for the benefit of faculty and field engineers. He served the institute as Associate Dean Academic, Director/Coordinator AVRC and Coordinator Information Super Highway Centre. Presently, he is Head, Continuing Education Centre and Coordinator, Quality Improvement Program Centre. His areas of interest are Measurement and Instrumentation, Medical Instrumentation, Medical Image Processing, Digital Signal Processing and Telemedicine.

Suresh Chandra Saxena received his B.E. degree from Allahabad University in 1970, M.E. Electrical (Measurement & Instrumentation) Hons and Ph.D. degree with specialization in Biomedical Engineering from Indian Institute of Technology Roorkee (erstwhile University of Roorkee) in 1973 and 1977 respectively. He joined as faculty in Electrical Engineering Department, Indian Institute of Technology Roorkee in 1973. After serving for 29 years at IIT Roorkee, he moved to Patiala and served as the Director, Thapar Institute of Engineering & Technology (TIET), Patiala from June 2002 to May 2006 and also the Director, Thapar Centre for Industrial Research & Development (TCIRD), Patiala from January 2004 to May 31, 2006. At present, he is the Director, Indian Institute of Technology Roorkee since June 01, 2006 and also mentor Director, IIT Mandi (HD), part time non official Director of Tehri Hydro Development Corporetion, Chairman of Northern-Region AICTE, Member of the executive Committee and Council of AICTE. He has more than 36 years of teaching, research and administrative experience. During this period, he has guided 25 PhDs and guiding 02 PhDs; guided 75 ME and more than 100 undergraduate students for their thesis and projects. He has published over 200 research papers in reputed national and international journals and conferences; written six monographs, organized/mentored 28 conferences; and edited 05 conference proceedings, organized 25 specialized courses for industry and handled 10 sponsored research schemes. His areas of specialization are Electrical Engineering, Biomedical Engineering and Instrumentation. He is fellow of The Institution of Engineers (India) {IE(I)}, fellow of Institution of Electronics and Telecommunication Engineers (IETE), and life member of Biomedical Engineering Society of India (BMESI), National Institution for Quality & Reliability (NIQR), Indian Society for Technical Education (ISTE) and Indian Society for Continuing Engineering Education (ISCEE). He has received 15 awards/honours including Khosla Gold Medal and cash award (two times), President of India's Prize, Jawaharlal Memorial Award, K.F. Antia Memorial Prize, Sir Thomas Ward Memorial Prize, K.S. Krishnan Memorial Award, honoured in October 2006 as "Outstanding Technologist" for the year 2006 by Punjab Technical University for outstanding contributions to technical education; honoured "Pride of Uttaranchal" award on 25th November 2006 by Dehradun Citizen's Council; and honoured by "Uttrakhand Ratan" – on 20th April 2008 by the All India Conference of Intellectuals, and The corps of Engineers Award of the IETE. He has been/is Chairman/President/Vice-Chairman/Vice-President/Member of a large number of Professional Societies, Board of Governors, Governing Councils, Executive Committees, Academic Councils, Assessment and Accreditation Committees, Administrative Bodies at national levels and effectively contributed in planning, development and monitoring of higher technical education in the country.

Dr. Niranjan Khandelwal did his M.B.B.S., from Calcutta University in 1980, postgraduate studies in Radiodiagnosis from Postgraduate Institute of Medical Education & Research, Chandigarh in 1984, diplomate N.B.E. in Radiodiagnosis at National Board of Examination, New Delhi in 1987 and F.I.C.R. at Indian College of Radiology & Imaging, New Delhi in 2005. His WHO fellowship in Neuroradiology at MGH, Boston and Mayo Clinic, Rochester in 1994.He is Professor & Head, Department of Radiodiagnosis, Postgraduate Institute of Medical Education & Research, Chandigarh since 2006. He has published 140 research papers and has contributed 15 chapters in books. He is Co-Editor of the Diagnostic Radiology-Neuroradiology including Head & Neck Imaging (ed) – 1999, Jaypee Brothers, Delhi. He is a life member of Indian College of Radiology & Imaging, Indian Radiological & Imaging Association, Neurological Society of India, Indian Academy of Neurology, Indian Society of Neuroradiology, Indian Society of Vascular & Interventional Radiology, Indian Federation of Ultrasound in Medicine & Biology, Indian Society of Paediatrics, and Indian Stroke Association. He has been President of Punjab and Chandigarh Branch of IRIA and Vice President of Indian Society of Vascular and Interventional Radiology. He is Honorary Secretary of Indian Society of Neuro Radiology since 2002 and President of Chandigarh Radiological Association since 2003.